J. Biochem. 2012;151(6):589–592 doi:10.1093/jb/mvs051

JB THE JOURNAL OF BIOCHEMISTRY

Rapid communication

Crystal structure of mitochondrial quinol–fumarate reductase from the parasitic nematode *Ascaris suum*

Received April 18, 2012; accepted May 1, 2012; published online May 9, 2012

Hironari Shimizu[1], Arihiro Osanai[1], Kimitoshi Sakamoto[1], Daniel Ken Inaoka[1], Tomoo Shiba[2], Shigeharu Harada[2,*] and Kiyoshi Kita[1,†]

[1]Department of Biomedical Chemistry, Graduate School of Medicine, University of Tokyo, 7-3-1 Hongo, Bunkyo-ku, Tokyo 113-0033; and [2]Department of Applied Biology, Graduate School of Science and Technology, Kyoto Institute of Technology, Sakyo-Ku, Kyoto 606-8585, Japan

*Shigeharu Harada, Department of Applied Biology, Graduate School of Science and Technology, Kyoto Institute of Technology, Sakyo-ku, Kyoto 606-8585, Japan. Tel: +81-75-724-7541; Fax: +81-75-724-7541, email: harada@kit.ac.jp

†Kiyoshi Kita, Department of Biomedical Chemistry, Graduate School of Medicine, University of Tokyo, 7-3-1 Hongo, Bunkyo-ku, Tokyo 113-0033, Japan. Tel: +81-3-5841-3526, Fax: +81-3-5841-3444, email: kitak@m.u-tokyo.ac.jp

In the anaerobic respiratory chain of the parasitic nematode *Ascaris suum*, complex II couples the reduction of fumarate to the oxidation of rhodoquinol, a reverse reaction catalyzed by mammalian complex II. In this study, the first structure of anaerobic complex II of mitochondria was determined. The structure, composed of four subunits and five co-factors, is similar to that of aerobic complex II, except for an extra peptide found in the smallest anchor subunit of the *A. suum* enzyme. We discuss herein the structure–function relationship of the enzyme and the critical role of the low redox potential of rhodoquinol in the fumarate reduction of *A. suum* complex II.

Keywords: *Ascaris suum*/crystal structure/mitochondrial respiratory complex II/rhodoquinol–fumarate reductase (QFR)/reaction mechanism.

Abbreviations: $C_{10}M$, *n*-decyl-β-D-maltoside; $C_{12}M$, *n*-dodecyl-β-D-maltoside; C_nE_m, *n*-alkyl ethylene glycol monoether; CybL, cytochrome *b* large subunit of complex II; CybS, cytochrome *b* small subunit of complex II; FAD, flavin adenine dinucleotide; Fp, flavoprotein subunit; Ip, iron–sulphur subunit; NADH, nicotinamide adenine dinucleotide; PEG, polyethyleneglycol; QFR, quinol–fumarate reductase; RQ, rhodoquinone; RQH_2, rhodoquinol; SML, sucrose monolaurate; SQR, succinate–ubiquinone reductase.

The anaerobic respiratory chain, known as the NADH-fumarate reductase (NADH-FRD) system, plays an essential role in the anaerobic energy metabolism of adult *Ascaris suum*, a parasite that inhabits the small intestine, an environment with low oxygen tension (pO_2 of ~4 mmHg). The NADH-FRD system comprises two membrane proteins, complexes I and II, embedded in the mitochondrial inner membrane. Complex I (NADH–rhodoquinone reductase) reduces rhodoquinone (RQ) to rhodoquinol (RQH_2) using the reducing equivalent of NADH, and complex II, which functions as a RQH_2–fumarate reductase (QFR), couples the reduction of fumarate to succinate to the oxidation of RQH_2 to RQ, a reverse reaction catalysed by mammalian complex II (succinate–ubiquinone reductase, SQR) of the aerobic respiratory chain. The anaerobic NADH-fumarate reductase system is found not only in *A. suum* but also in bacteria and many other parasites, and is thus a promising target for chemotherapy (*1-3*).

Although no structure is currently available for eukaryotic QFR-type complex II, structures of SQR-type complex II from porcine (*4*), avian (*5*) and *Escherichia coli* (*6*), as well as those of QFR-type from *E. coli* (*7*) and *Wolinella succinogenes* (*8*), have been determined. Their structures are similar to each other and are generally composed of four polypeptides, the largest flavoprotein subunit (Fp, 70 kDa), an iron–sulphur cluster subunit (Ip, 30 kDa), and cytochrome *b* large (CybL, 15 kDa), and small (CybS, 13 kDa) subunits. In this study, the first X-ray structural analysis of a eukaryotic QFR-type complex II was performed for *A. suum* adult complex II (*A. suum* QFR) in order to clarify the factors responsible for its QFR activity and the mechanisms of RQH_2 oxidation coupled to fumarate reduction.

Ascaris suum QFR was extracted and purified from adult *A. suum* muscle mitochondria and crystallized according to the method described by Osanai *et al.* (*9*). In brief, ~4 kg of *A. suum* obtained from a local slaughterhouse was minced and suspended in Chappell-Perry medium (100 mM KCl, 50 mM Tris–HCl pH 7.4, 5 mM magnesium sulphate, 1 mM ATP, 1 mM EDTA). The fraction containing mitochondria was separated by differential centrifugation, and *A. suum* QFR was then solubilized using 1.0% (w/v) sucrose monolaurate (SML; Dojindo). After purification with anion-exchange column chromatography, SML was exchanged with a mixture of octaethylene glycol monododecyl ether ($C_{12}E_8$) and dodecyl maltoside ($C_{12}M$) by repeated PEG3350 precipitation and dissolution in a buffer containing 0.6% (w/v) $C_{12}E_8$, 0.4% (w/v) $C_{12}M$, 200 mM NaCl, 10 mM Tris–HCl pH 7.5 and 1 mM sodium malonate. Crystallization was performed by the dialysis method using a reservoir solution containing 15% (w/v) PEG3350, 100 mM Tris–HCl pH 8.4, 200 mM NaCl,

1 mM sodium malonate, 0.06% (w/v) $C_{12}E_8$ and 0.04% (w/v) $C_{12}M$. Reddish crystals grew to 100–200 μm in 2–3 days. Crystals of *A. suum* QFR in complex with fumarate were prepared by soaking crystals in the reservoir solution supplemented with 1 mM of sodium fumarate instead of sodium malonate.

X-ray diffraction experiments were performed under a N_2 gas stream (100 K) at SPring-8 beam line BL44XU (Bruker DIP-6040 detector) and at Photon Factory beam line NW12 (ADSC315 CCD detector). Data were processed and scaled using *HKL2000* (*10*). The initial structural model of *A. suum* QFR was solved by molecular replacement using the structure of porcine complex II (pdb code: 1ZOY) as a search model. *Molrep* (*11*) was used for molecular replacement. The refinement of the structure and model building were performed using *Refmac5* (*12*) and *Coot (13*), respectively. Data processing and refinement statistics are shown in Supplementary Table SI. All figures were generated using *PyMOL* (*14*). The coordinates have been deposited in the Protein Data Bank under ID codes 3VR8 and 3VRB for the malonate and fumarate bound forms, respectively.

The X-ray structure of *A. suum* QFR (Fig. 1A and B) is composed of Fp, Ip, CybL and CybS subunits, with two molecules in the asymmetric unit (chains A–D and E–H, respectively). As there are no significant differences between the overall protein structures of 3VR8 and 3VRB, we will focus on chains A–D of the malonate-bound form to describe the protein structure as a whole. Fp (chain A) and Ip (chain B) are hydrophilic, whereas CybL (chain C) and CybS (chain D) are hydrophobic membrane-integrated subunits. Fp comprises four domains: a FAD binding domain (residues A33–A279 and A384–A465), a capping domain (A279–A384), a helical domain (A465–A580) and a C-terminal domain (A580–A645). A FAD prosthetic group is held in the FAD binding domain by a covalent bond to His A79 and by hydrogen bonds with highly conserved residues (Ala A49, Thr A71, Lys A72, Met A73, Ser A78, Thr A80, Gln A84, Gly A85, Gly A86, Ala A201, Asp A255, Glu A421, Arg A432, Ser A437, Leu A438) across amino acid sequences of complex IIs from various species. Ip contains an N-terminal plant ferredoxin-like domain (residues B33–B130) and a C-terminal bacterial ferredoxin-like domain (B130–B281). Of the three iron–sulphur centres bound to Ip, [2Fe–2S] is coordinated by four cysteine residues (B89, B94, B97 and B109) and located in the N-terminal domain, whereas [4Fe–4S] and [3Fe–4S] that are coordinated by four (B182, B185, B188 and B249) and three (B192, B239 and B245) cysteine residues, respectively, are bound to the C-terminal domain. These iron–sulphur centres are also surrounded with highly conserved hydrophobic amino acid residues (Fig. 1C). The structures of Fp and Ip are similar to those of complex IIs with known structures, such as *E. coli* SQR (*6*), *E. coli* QFR (*7*), *W. succinogens* QFR (*8*), porcine SQR (*4*) and avian SQR (*5*).

In contrast to Fp and Ip, the hydrophobic membrane-spanning part shows diversity among species. In *W. succinogens* QFR, it consists of a single polypeptide chain and two haem *b* prosthetic groups, whereas *A. suum* QFR, like *E. coli* SQR, porcine SQR and avian SQR, holds two polypeptide chains (CybL and CybS) and one haem *b*. Both CybL and CybS consist of three membrane-spanning α-helices

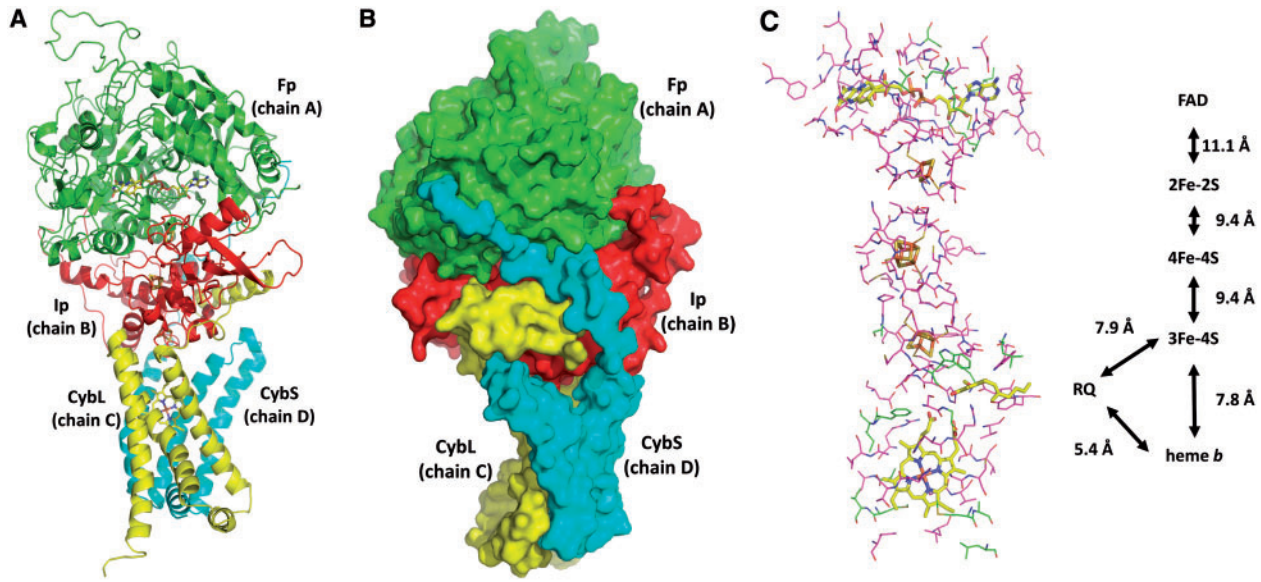

Fig. 1 Structure of *A. suum* QFR. Fp (chain A), Ip (chain B), CybL (chain C) and CybS (chain D) are coloured in green, red, yellow and cyan, respectively. Colour code for each atom type: C (yellow), N (blue), O (red), S (orange) and Fe (brown). (A) Cartoon representation of the *A. suum* QFR structure. FAD, iron–sulphur centres and haem *b* are shown as sticks. (B) Surface model of *A. suum* QFR viewed from a different direction from (A) for easy observation of the extra polypeptide attached to the N-terminus of CybS. (C) The arrangement of FAD, [2Fe–2S], [4Fe–4S], [3Fe–4S], haem *b* and RQ. Their edge-to-edge distances are also shown. Amino acid residues within 5 Å of the prosthetic groups and RQ are shown by a wire model. Conserved residues across amino acid sequences of complex IIs are coloured in magenta.

(Fig. 1A and B) and anchor the *A. suum* QFR to the membrane. A haem *b* is embedded into the interface between the CybL and CybS, and two conserved His residues (His C131 and His D95) are ligated to the haem iron. A distinct cleft, whose location is in agreement with the quinone binding sites proposed for other complex IIs, is formed by Ip, CybL and CybS, and a residual electron density probably revealing a bound RQ is detected in the cleft.

Figure 1C shows the arrangement of the prosthetic groups bound to *A. suum* QFR and their edge-to-edge distances. [2Fe–2S], [4Fe–4S] and [3Fe–4S] line between FAD and RQ as observed in other complex IIs (*15*). Thus, the disposition of the prosthetic groups is critical to allow electron transfer from RQH_2 to FAD via the iron–sulphur centres. The hydrophobic environment around the iron–sulphur centres and distances between neighbouring centres (<14 Å) suggest that the electron transfer from RQH_2 to FAD is carried out by quantum tunneling (*16*), as proposed for *E. coli* SQR (*6*).

Figure 2A shows that fumarate is bound near the FAD isoalloxazine ring in a non-planar conformation. C2, C3 and C4 carboxyl group are in the same plane parallel to the isoalloxazine ring, whereas the C1 carboxyl group is twisted around the C1 and C2 bond with a C3–C2–C1–O1A dihedral angle of 83.7°. The twisting, which is stabilized by hydrogen bonds with Gly A85, Thr A288, Glu A289 and Arg A320, suggests that the uniform distribution of π-electrons over the conjugated double bonds of fumarate is broken and a partial charge separation, $C2^{\delta+}$ and $C3^{\delta-}$, is induced. The contact of $C2^{\delta+}$ with FAD N5 (4.05 Å) suggests that a hydride (or hydride equivalent) is transferred from reduced FAD N5 to $C2^{\delta+}$ in the reduction of fumarate with the reduced FAD. Arg A320 is a probable candidate that supplies a proton to $C3^{\delta-}$ to complete the reduction of fumarate. The twisted conformation of fumarate is also observed in flavoproteins with fumarate reductase acitivity (1D4E, 1P2E, 1QLB and 2E6D), and a similar mechanism is proposed for *E. coli* QFR (*17*) and *Trypanosoma cruzi* dihydroorotate dehydrogenase (*18*).

Figure 2B shows the structure of the RQ binding site proposed for *A. suum* QFR. The site is formed by Ip, CybL and CybS, and is in agreement with ubiquinone binding sites suggested for other complex IIs. [3Fe–4S] is the nearest iron–sulphur centre to RQ (9.2 and 7.9 Å from RQ O1 and RQ O2, respectively), suggesting that electrons are first accepted by [3Fe–4S] upon the oxidization of RQH_2, and then transferred to FAD via [4Fe–4S] and [2Fe–2S].

RQ is surrounded by conserved amino acid residues (Ser C72, Arg C76, Asp D106 and Tyr D107) and is involved in hydrogen bond networks, RQ O1–Tyr D107–Arg C76–Asp D106 and RQ O2–Ser C72–RQ N–Arg C76–Asp D106. Protons abstracted from RQH_2 may leave along these networks. It should be noted that the amino group of RQ, which is replaced by the methoxy group in ubiquinone, is involved in one of the hydrogen bond networks.

In this study, the structure of *A. suum* QFR, the first structure of a mitochondrial QFR-type complex II, has been determined. A comparison of structures of *A. suum* QFR and SQR-type complex II reveals that not only are the protein structures essentially identical to each other, but also the bound prosthetic groups are surrounded by conserved residues (Fig. 1C). Thus, it appears that the bound quinone type plays a role in determining the direction of catalysis, QFR or SQR of complex II. In fact, *A. suum* QFR, which catalyses the reduction of fumarate ($Em' = +30$ mV) by oxidizing RQH_2 ($Em' = -63$ mV) *in vivo*, displays SQR activity,

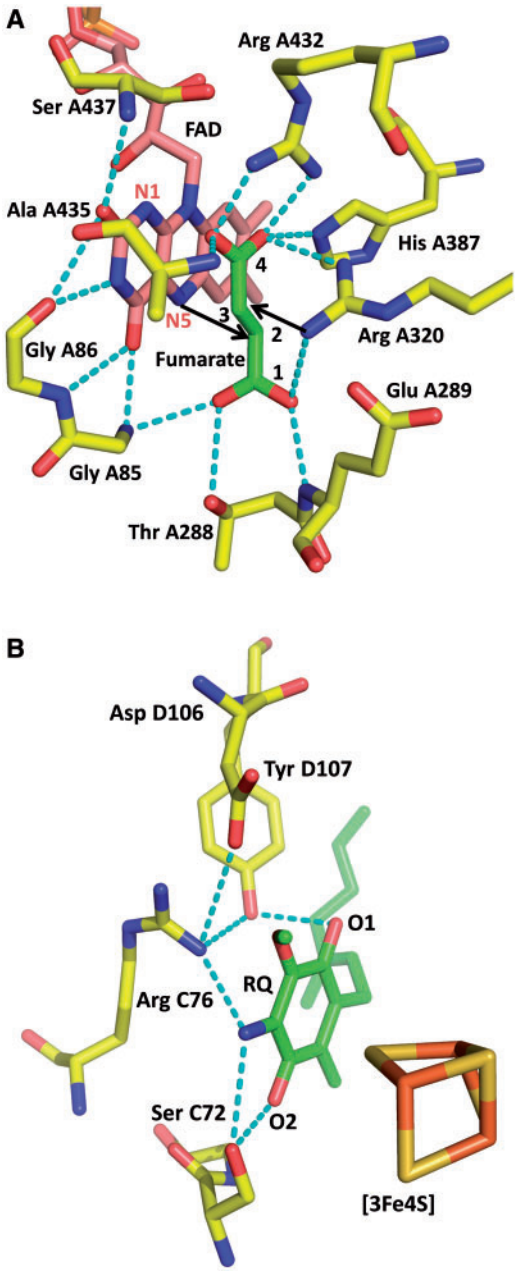

Fig. 2 Close-up views of active site structures of *A. suum* QFR. (A) Fumarate binding site of *A. suum* QFR. The C1 carboxyl group is twisted around the C1 and C2 bond by hydrogen bonds with nearby residues, which induces partial charge separation, $C2^{\delta+}$ and $C3^{\delta-}$. (B) RQH_2 binding site of *A. suum* QFR. Colour code for each atom type: C (yellow), N (blue), O (red), S (orange) and Fe (brown). Fumarate and RQ are coloured in green, FAD in pink. Hydrogen bonds are drawn with cyan dotted lines.

oxidation of succinate ($Em' = +30$ mV), and reduction of ubiquinol ($Em' = +110$ mV) *in vitro*.

The structure also demonstrates a feature unique to *A. suum* QFR. The additional polypeptide composed of 27 residues, which is found only at the N-terminus of *A. suum* CybS, extends to and forms hydrogen bonds with CybL, Ip and Fp (Fig. 1B, cyan), indicating that this unique region probably contributes to the stabilization of the *A. suum* QFR structure. In addition, because no such region has been found in SQR-type complex IIs known to date, this unique feature could make *A. suum* QFR favourable for accepting RQH_2 and fumarate as substrates, although further biochemical and biophysical analyses are necessary to reveal the truth.

Supplementary Data

Supplementary Data are available at *JB* Online.

Funding

This work was supported in part by Creative Scientific Research Grant 18GS0314 (to KK), Grant-in-aid for Scientific Research on Priority Areas 18073004 (to KK) and 19036010 (to SH) from the Japanese Society for the Promotion of Science, and Targeted Proteins Research Program (to KK and SH) from the Japanese Ministry of Education, Science, Culture, Sports and Technology (MEXT).

Conflict of interest

None declared.

References

1. Omura, S., Miyadera, H., Ui, H., Shiomi, K., Yamaguchi, Y., Masuma, R., Nagamitsu, T., Takano, D., Sunazuka, T., Harder, A., Kolbl, H., Namikoshi, M., Miyoshi, H., Sakamoto, K., and Kita, K. (2001) An anthelmintic compound, nafuredin, shows selective inhibition of complex I in helminth mitochondria. *Proc. Natl. Acad. Sci. USA* **98**, 60–62
2. Matsumoto, J., Sakamoto, K., Shinjyo, N., Kido, Y., Yamamoto, N., Yagi, K., Miyoshi, H., Nonaka, N., Katakura, K., Kita, K., and Oku, Y. (2008) Anaerobic NADH-fumarate reductase system is predominant in the respiratory chain of *Echinococcus multilocularis*, providing a novel target for the chemotherapy of alveolar echinococcosis. *Antimicrob. Agents Chemother.* **52**, 164–170
3. Sakai, C., Tomitsuka, E., Esumi, H., Harada, S., and Kita, K. (2012) Mitochondrial fumarate reductase as a target of chemotherapy: from parasites to cancer cells. *Biochim. Biophys. Acta* **1820**, 643–651
4. Sun, F., Huo, X., Zhai, Y., Wang, A., Xu, J., Su, D., Bartlam, M., and Rao, Z. (2005) Crystal structure of mitochondrial respiratory membrane protein complex II. *Cell* **121**, 1043–1057
5. Huang, L.S., Sun, G., Cobessi, D., Wang, A.C., Shen, J.T., Tung, E.Y., Anderson, V.E., and Berry, E.A. (2006) 3-Nitropropionic acid is a suicide inhibitor of mitochondrial respiration that, upon oxidation by complex II, forms a covalent adduct with a catalytic base arginine in the active site of the enzyme. *J. Biol. Chem.* **281**, 5965–5972
6. Yankovskaya, V., Horsefield, R., Tornroth, S., Luna-Chavez, C., Miyoshi, H., Leger, C., Byrne, B., Cecchini, G., and Iwata, S. (2003) Architecture of succinate dehydrogenase and reactive oxygen species generation. *Science* **299**, 700–704
7. Iverson, T.M., Luna-Chavez, C., Cecchini, G., and Rees, D.C. (1999) Structure of the *Escherichia coli* fumarate reductase respiratory complex. *Science* **284**, 1961–1966
8. Lancaster, C.R., Kroger, A., Auer, M., and Michel, H. (1999) Structure of fumarate reductase from *Wolinella succinogenes* at 2.2 Å resolution. *Nature* **402**, 377–385
9. Osanai, A., Harada, S., Sakamoto, K., Shimizu, H., Inaoka, D.K., and Kita, K. (2009) Crystallization of mitochondrial rhodoquinol-fumarate reductase from the parasitic nematode *Ascaris suum* with the specific inhibitor flutolanil. *Acta Crystallogr. Sect. F Struct. Biol. Cryst. Commun.* **65**, 941–944
10. Otwinowski, Z. and Minor, W. (1997) Macromolecular crystallography part A [20] Processing of X-ray diffraction data collected in oscillation mode. *Methods Enzymol.* **276**, 307–326
11. Vagin, A. and Teplyakov, A. (2010) Molecular replacement with *MOLREP*. *Acta Crystallogr. D Biol. Crystallogr.* **66**, 22–25
12. Murshudov, G.N., Vagin, A.A., and Dodson, E.J. (1997) Refinement of macromolecular structures by the maximum-likelihood method. *Acta Crystallogr. D Biol. Crystallogr.* **53**, 240–255
13. Emsley, P. and Cowtan, K. (2004) *Coot*: model-building tools for molecular graphics. *Acta Crystallogr. D Biol. Crystallogr.* **60**, 2126–2132
14. DeLano, W.L. (2002) *The PyMOL Molecular Graphics System*. DeLano Scientific LLC, Palo Alto, California, USA
15. Horsefield, R., Iwata, S., and Byrne, B. (2004) Complex II from a structural perspective. *Curr. Protein Pept. Sci.* **5**, 107–118
16. Page, C.C., Moser, C.C., Chen, X., and Dutton, P.L. (1999) Natural engineering principles of electron tunnelling in biological oxidation-reduction. *Nature* **402**, 47–52
17. Tomasiak, T.M., Archuleta, T.L., Andrell, J., Luna-Chavez, C., Davis, T.A., Sarwar, M., Ham, A.J., McDonald, W.H., Yankovskaya, V., Stern, H.A., Johnston, J.N., Maklashina, E., Cecchini, G., and Iverson, T.M. (2011) Geometric restraint drives on- and off-pathway catalysis by the *Escherichia coli* menaquinol:fumarate reductase. *J. Biol. Chem.* **286**, 3047–3056
18. Inaoka, D.K., Sakamoto, K., Shimizu, H., Shiba, T., Kurisu, G., Nara, T., Aoki, T., Kita, K., and Harada, S. (2008) Structures of *Trypanosoma cruzi* dihydroorotate dehydrogenase complexed with substrates and products: atomic resolution insights into mechanisms of dihydroorotate oxidation and fumarate reduction. *Biochemistry* **47**, 10881–10891